JGR Atmospheres

RESEARCH ARTICLE
10.1029/2019JD032100

The Evolving Distribution of Relative Humidity Conditional Upon Daily Maximum Temperature in a Warming Climate

Jiacan Yuan[1,2,3], **Michael L. Stein**[3,4,5], **and Robert E. Kopp**[2,3]

[1]Department of Atmospheric and Oceanic Sciences and Institute of Atmospheric Sciences and Big Data Institute for Carbon Emission and Environmental Pollution, Fudan University, Shanghai, China, [2]Department of Earth and Planetary Sciences, Rutgers University, New Brunswick, NJ, USA, [3]Rutgers Institute of Earth, Ocean, and Atmospheric Sciences, Rutgers University, New Brunswick, NJ, USA, [4]Department of Statistics, University of Chicago, Chicago, IL, USA, [5]Department of Statistics, Rutgers University, New Brunswick, NJ, USA

Abstract The impacts of heat waves in a warming climate depend not only on changing temperatures but also on changing humidity. Using 35 simulations from the Community Earth System Model Large Ensemble (CESM LENS), we investigate the long-term evolution of the joint distribution of summer relative humidity (RH) and daily maximum temperature (*Tmax*) near four U.S. cities (New York City, Chicago, Phoenix, and New Orleans) under the high-emissions Representative Concentration Pathway (RCP) 8.5. We estimate the conditional quantiles of RH given *Tmax* with quantile regression models, using functions of temperature for each city in July for three time periods (1990–2005, 2026–2035, and 2071–2080). Quality-of-fit diagnostics indicate that these models accurately estimate conditional quantiles for each city. As expected, each quantile of *Tmax* increases from 1990–2005 to 2071–2080, while mean RH decreases modestly. Conditional upon a fixed quantile of *Tmax*, the median and high quantiles of RH decrease, while those of the Heat Index (HI) and dew point both increase. This result suggests that, despite a modest decrease in median relative humidity, heat stress measured by metrics considering both humidity and temperature in a warming climate will increase faster than that measured by temperatures alone would indicate. For a fixed *Tmax*, the high quantiles of RH (and thus of HI and dew point) increase from 1990–2005 to 2071–2080 in all four cities. This result suggests that the heat stress of a day at a given *Tmax* will increase in a warming climate due to the increase of RH.

Key Points:
- The quantile-regression models accurately estimate the conditional distribution of relative humidity given temperature
- Incorporating the effect of relative humidity, heat stress in a warming climate will increase faster than temperatures alone would indicate
- The heat stress of a day at a fixed daily maximum temperature will increase due to the increase of relative humidity as climate warms

Supporting Information:
- Supporting Information S1

Correspondence to:
J. Yuan,
jcyuan@fudan.edu.cn

Citation:
Yuan, J., Stein, M. L., & Kopp, R. E. (2020). The evolving distribution of relative humidity conditional upon daily maximum temperature in a warming climate. *Journal of Geophysical Research: Atmospheres*, *125*, e2019JD032100. https://doi.org/10.1029/2019JD032100

Received 27 NOV 2019
Accepted 30 AUG 2020
Accepted article online 8 SEP 2020

Author Contributions:
Conceptualization: Jiacan Yuan, Michael L. Stein, Robert E. Kopp
Funding acquisition: Robert E. Kopp
Investigation: Jiacan Yuan
Methodology: Jiacan Yuan, Michael L. Stein
Validation: Jiacan Yuan, Michael L. Stein
Visualization: Jiacan Yuan
Writing - original draft: Jiacan Yuan
Writing – review & editing: Michael L. Stein, Robert E. Kopp

1. Introduction

Heat waves, events in which unseasonably hot weather lasts days to weeks, negatively impact human health, ecosystems, crop yields, and physical infrastructure (Allen et al., 2010; Fontana et al., 2015; Ramamurthy et al., 2017; Zuo et al., 2015). As the climate continues to warm, heat waves are projected to increase in frequency and duration (Collins et al., 2013; Meehl & Tebaldi, 2004; Papalexiou et al., 2018). In addition, the portion of the world's population and land area that are exposed to deadly heat (referring to extremely hot conditions that may cause death) is projected to increase even under a scenario with aggressive mitigation of greenhouse gas emissions (Li et al., 2020; Mora et al., 2017). Thus, climate change raises serious concerns on the growing impact of heat waves (Stocker et al., 2013).

Although many studies have targeted heat waves and their impact on human health (Basu & Samet, 2002; Mazdiyasni et al., 2017; Meehl & Tebaldi, 2004; Mora et al., 2017; Orlowsky & Seneviratne, 2012; Tebaldi et al., 2006), there is still debate on the most appropriate ways to identify extreme values of heat for the assessment of heat-related mortality and illness. Much of the literature only uses temperature to describe heat extremes (Carleton et al., 2020; Dosio et al., 2018; Kodra & Ganguly, 2014; Mazdiyasni et al., 2017; Meehl & Tebaldi, 2004; Tebaldi et al., 2006). However, other climate variables (e.g., humidity, solar radiation, and wind speed) may also contribute to human discomfort and mortality. Mora et al. (2017) assessed multiple pairs of climate variables: surface temperature, relative humidity (RH), solar radiation, and wind speed. They found the pair combining surface temperature and RH most accurately identifies lethal

conditions. High humidity is an important contributor to heat stress, as it can reduce the human body's capability to remove metabolic heat by sweating.

An increasing number of studies consider both temperature and humidity to identify the extreme value of heat (Buzan et al., 2015; Dunn et al., 2014; Fischer et al., 2012; Li et al., 2020; Willett & Sherwood, 2012; Oleson et al.,2013). Fischer and Knutti (2013) suggested that the quantities jointly defined by temperature and RH can reduce uncertainty of future projections of heat extremes. There are many metrics that use temperature and humidity to measure heat stress and thermal comfort (Willett & Sherwood, 2012). The Temperature-Humidity Index (THI) is a common measure of heat stress initially developed for humans (Thom, 1958) and was extended to assess thermal response of dairy cattle (Berry et al., 1964; Dunn et al., 2014). The Heat Index (HI), which is broadly used in weather warning systems for heat stress, can be estimated by a multiple-regression model of temperature and RH (Rothfusz, 1990). The simplified Wet-Bulb Globe Temperature (sWBGT) (Iribarne & Godson, 1981) is another widely used metric that represents heat stress for an outdoor condition assuming moderately high radiation levels and light wind conditions. Humidex (HUMIDEX) was developed to describe the feels-like temperature for humans (Masterton & Richardson, 1979). Russo et al. (2017) introduced a new Apparent Heat Wave Index (AHWI) that utilizes both daily maximum temperature and daily minimum RH to define heat waves and physiologic stress. In addition, some other metrics include effects from not only temperature and humidity but also from wind and solar radiation, such as the Apparent Temperature (Steadman, 1979a, 1979b), Environmental stress index (Moran et al., 2001), and Wet-Bulb Globe Temperature (Yaglou & Minard, 1957).

In the context of global warming, the long-term trend of land surface temperature is positive in both present observations and future projections (Byrne & O'Gorman, 2018; Dai, 2006; Sutton et al., 2007). Although the specific humidity increases as climate warms (Stocker et al., 2013), a decrease in surface RH over land has been observed since 2000. In situ observations show that RH averaged over land decreased from 2000 but had not recovered as of 2018 (Byrne & O'Gorman, 2018; Willett et al., 2014; 2018). The decline in land-averaged RH since 2000 is also observed in reanalysis data, where the decrease in RH is greater than that from in situ observations (Dunn et al., 2017; Willett et al., 2018). Although this observed decline of land-averaged RH since 2000 is not captured by some global climate models in the Coupled Model Intercomparison Project Phase 5 (CMIP5) archive (Dunn et al., 2017), the multimodel annual mean projects that surface RH will decrease over most land areas (except for parts of tropical Africa and South Asia) by the end this century, possibly due to the faster increase in surface air temperature over land than over the ocean (Byrne & O'Gorman, 2016; Kirtman et al., 2013). Given projected increases in temperature and decreases in RH, the evolution of the RH distribution conditional on temperature and its contribution to future heat extremes is not well understood. In this study, we use both temperature and RH as contributing variables to identify heat extremes and investigate the long-term evolution of their joint distribution.

Conventional approaches assessing extreme events may apply an assumption about the tail of the distribution of the contributing variable (e.g., Kharin et al., 2013; Kodra & Ganguly, 2014) and assume only the parameters of the presumed distribution change as the climate gets warmer. However, the distributions of these contributing variables generally do not follow a standard distribution. Furthermore, shapes of distributions may change quite substantially in a warming climate (Haugen et al., 2018). In this study, we develop a statistical model to characterize the distribution of RH conditional on daily maximum temperature (*Tmax*), as well as its evolution, without assuming any particular parametric form for this distribution. In addition, our approach provides a representation of RH distribution conditional on continuous *Tmax*, rather than breaking the data set into *Tmax* bins, and can estimate the tails making the best use of the available information. To reach this end, we applied quantile regression to the Community Earth System Model Large Ensemble (LENS, Kay et al., 2015), which provides a sufficient volume of samples to allow accurate estimation for the tails of the distribution of a climate variable (Haugen et al., 2018).

Quantile regression is a form of regression analysis that estimates conditional quantile functions—models in which, for any given quantile (τ) between 0 and 1, the τ^{th} conditional quantile of the response variable is expressed as a linear function of predictor variables (Koenker & Hallock, 2001), where the coefficients in this linear function can vary with τ. Haugen et al. (2018) applied quantile regression to temperature in an ensemble of simulations from CESM (Sriver et al., 2015) to study the evolving distribution of temperature in a warming climate. They constructed a quantile regression model that continuously represents the smooth

evolution of temperature distributions both day to day over an annual cycle and year to year over longer temporal trends over North America. Quantile regression provides a natural way to study the nuanced changes in distributions, especially their tails, which are essential for studies of weather extremes. Haugen et al. (2018) used temperature as the response and function of days in a year and years as predictors. Here, we focus on using functions of temperature as predictors for RH. Estimating the distribution of RH conditional on *Tmax* (RH|*Tmax*) provides flexibility for quantifying heat extremes by RH and *Tmax* simultaneously. This approach allows us to look at RH at a given temperature or RH at given temperature quantile. In addition, it allows us to assess any variables that take both temperature and RH into account, such as dew point, HI, and wet bulb temperature.

We developed models for four major U.S. cities (Figure S1 in supporting information) in different climate settings: New York City (NYC) has a humid temperate climate; Chicago (CHI) has a hot-summer humid continental climate; Phoenix (PHX) has a hot-desert climate; and New Orleans (NOLA) has a humid subtropical climate. These four cities were selected to test the sensitivity of the approach in a variety of climates. Our approach can be applied to different locations with different climate backgrounds.

Section 3 describes the data sources used in this study, as well as the approaches used to calculate key metrics. Section 4 numerically diagnoses the joint distribution of RH and *Tmax*, identifying features used to help select the form of basis functions used in the statistical models. Section 5 describes the statistical methodology. Section 6 presents the approaches used to validate the quality of fit of the statistically estimated quantiles. Section 7 presents key results, including the estimated quantiles of RH|*Tmax* and discusses the implications of the estimated quantiles of RH|*Tmax* for extreme heat in future projections. Section 7 provides conclusions and discussions. Details on the selection of basis functions for the statistical models are described in the appendix.

2. Data Sources and Meteorological Metrics

2.1. Data

The CESM LENS provides sufficiently large samples to yield accurate estimates of conditional quantiles via quantile regression. The LENS data set is a 40-member initial-conditions ensemble forced by Representative Concentration Pathway (RCP) 8.5, which represents a high-emissions scenario in which emissions continue to rise through the 21st century (van Vuuren et al., 2011). Of the 40 ensemble members, 35 were run on the Yellowstone supercomputer, while the other 5 members were run on University of Toronto supercomputer. We used the 35 members obtained from the same machine. The principal variables used in this study were 6-hourly surface temperature (TREFHT) and 6-hourly surface specific humidity (QREFHT, kg/kg). These 6-hourly data with a horizontal resolution of 0.94° × 1.25° are only available for three periods: 1990–2005, 2026–2035, and 2071–2080 (URL of the data:

https://www.earthsystemgrid.org/dataset/ucar.cgd.ccsm4.CESM_CAM5_BGC_LE.atm.proc.6hourly_inst.html). We extract the *Tmax* based on the 6-hourly data. We use 6-hourly data as a compromise in practice because it is the highest temporal resolution of LENS output. Note here the *Tmax* we obtained is likely to underestimate the true *Tmax* of a day, as the 6-hourly frequency may miss the peak of temperature in a diurnal cycle. RH was determined from the specific humidity q and surface pressure P at the time at which the *Tmax* was observed (Lawrence, 2005) using

$$RH = \frac{q}{q_{sat}} = \frac{q\,(P - e_{sat})}{0.622 \times e_{sat}}, \tag{1}$$

$$e_{sat} = C \exp\left(\frac{A\ Tmax}{Tmax + B}\right), \tag{2}$$

where $A = 17.625$, $B = 243.04$°C, and $C = 610.94$°C. These coefficients are taken from Alduchov and Eskridge (1996), who recommend that Equation 2 provides an estimate of e_{sat} with a relative error of <0.4% over the range -40°C $\leq Tmax \leq 50$°C.

We select four grid cells corresponding to the four focal cities (Figure S1): (41.00°N, 73.75°W) for NYC, (41.00°N, 271.25°W) for CHI, (29.69°N, 270.00°W) for NOLA, and (33.46°N, 247.50°W) for PHX. Note that

we use a grid cell southwest of the urban area of Chicago to represent CHI. The urban Chicago cell, of which Lake Michigan comprises about half, produces some extremely hot and humid days, for which the corresponding heat indices in the period of 1990–2005 are substantially higher than the historical record at Chicago (Figure S2). This mismatch may arise due to the poor representation of Lake Michigan in CESM (Subin et al., 2012) and motivates our choice of a more inland cell.

The CESM has an urban model, which can simulate the urban climate at subgrid scales (Fischer et al., 2012; Oleson et al., 2013). However, the LENS data we used in this study are output based on the standard CESM grid box, which is larger than the subgrid scale. Therefore, data at a grid cell are a mix of signals calculated over an urban tile and mainly rural plant functional types at subgrid scales. Although we use the city name to label the four grid cells, climate data at each cell are more representative for the rural climate around that city than the urban climate of the city.

To validate the model data with historical observational data, we use Version 3.0.0.2018f of the Hadley Centre Global Sub-Daily Station Observation (HadISD) air temperature and dew point temperature (https://www.metoffice.gov.uk/hadobs/hadisd/v300_2018f/index.html). HadISD is a quality controlled global subdaily data set that contains weather data at the station level (Dunn et al., 2012). HadISD has hourly temporal resolution but was converted to 6-hourly data by taking the instantaneous temperature and dew point temperature (T_d) at 0:00, 6:00, 12:00, and 18:00 of the Coordinated Universal Time, to be consistent with the LENS data. Then, we select *Tmax* based on the 6-hourly data and the dew point temperature (T_d) from the time when the *Tmax* is selected. The RH is obtained from *Tmax* and the corresponding T_d (Lawrence, 2005):

$$RH = \exp\left(A\left(\frac{T_d}{T_d + B} - \frac{Tmax}{Tmax + B}\right)\right). \tag{3}$$

2.2. Computation of Meteorological Metrics

The dew point temperature (T_d) is the temperature at which an air particle reaches saturation by cooling the air isobarically. We use an empirical method, the Magnus formula, (Alduchov & Eskridge, 1996; Gibbins, 1990) to calculate T_d from *RH* and *Tmax*.

$$T_d = \frac{B\gamma}{A - \gamma}, \tag{4}$$

$$\gamma = \ln RH + A\frac{Tmax}{Tmax + B}. \tag{5}$$

The A and B in Equations 3–5 are the same with the A and B in Equation 2.

The U.S. National Weather Service (NWS) uses the HI in their heat stress early warning system. Similarly, we use the empirical equation developed by Rothfusz (1990), who performed a multiple regression analysis on the data of HI from Steadman's comfort model (Steadman, 1979a), which considers 15 parameters including vapor pressure, surface temperature, effective wind speed, and other parameters related to physiology, clothing, and heat-transfer basis of human. The formula of Rothfusz equation we used in this study is (Rothfusz, 1990):

$$\begin{aligned} HI = {} & -42.379 + 2.04901523 \times Tmax + 10.14333127 \times RH \\ & - 0.22475541 \times Tmax \times RH - 6.83783 \times 10^{-3} \times Tmax^2 - 5.481717 \times 10^{-2}\mathrm{R}^2 \\ & + 1.22874 \times 10^{-3} \times Tmax^2 \times RH + 8.5282 \times 10^{-4} \times Tmax \times R^2 \\ & - 1.99 \times 10^{-6} \times Tmax^2 \times R^2, \end{aligned}$$

where *HI* is in units of degrees Fahrenheit. We then convert this index to degrees Celsius to keep the units consistent with *Tmax* and T_d. Although only temperature and humidity are used as predictors in the regression analysis, other parameters in Steadman's comfort model are assumed to be within the regression coefficients of Equation 6. Following the instructions of the Weather Prediction Center of NWS in United States (https://www.wpc.ncep.noaa.gov/html/heatindex_equation.shtml), we apply adjustments to the HI if the *Tmax* and RH are in some specific ranges. As Equation 6 is established based on the

data from Steadman's tables (Steadman, 1979a, 1979b), it is not valid for temperature that are out of the range of data considered by Steadman (i.e., 20–50°C). Most of *Tmax* used in this study is below the upper boundary except for some days in PHX during the period of 2071–2080, when the *Tmax* is greater than 50°C. We should interpret these HI obtained when *Tmax* is larger than 50°C with caution when investigating the heat stress based on HI.

The enthalpy of air (E), which is the sum of its sensible and latent heat, is suggested to constrain the upper bound of heat stress indices considering both temperature and humidity (Fischer & Knutti, 2013; Matthews, 2018). We calculate E based on *Tmax*, *RH*, and P at the same hour when *Tmax* was observed:

$$E = Tmax \times C_p + q \times L, \tag{7}$$

$$= Tmax \times C_p + RH \times \frac{e_{sat} \times 0.622}{P - e_{sat}} \times L, \tag{8}$$

where $C_p = 1{,}005.7\ \mathrm{J\ kg^{-1}{}^{\circ}C^{-1}}$ is the specific heat capacity of air at constant pressure for air temperature between −100°C and 100°C. The factor L represents the latent heat of evaporation. As temperature varies within a small range, here we assume L is a constant with a value of 2.5×10^6 J/kg (Yano & Ambaum, 2017). e_{sat} is the saturated vapor pressure, which is expressed in Equation 2.

3. Joint Distribution Between RH and *Tmax*

To determine the form of basis functions used in the statistical models, we examine numerically the joint distribution of RH and *Tmax* for three different periods at four cities in July (Figure 1). From 1990–2005 to 2071–2080, the shapes of the joint distributions in each city are generally preserved, but, as expected, distributions shift toward hotter temperature. For all four cities, a fairly sharp upper boundary curve exists with many data from LENS just to the left of the curve (cooler and less humid) and very few to its right (hotter and more humid).

This cutoff may reveal a constraint on moist enthalpy controlled by local meteorological conditions (Fischer & Knutti, 2013; Matthews, 2018). The enthalpy is low when both *Tmax* and RH are low and reaches its observed maximum near the cutoff (Figure 1). As the variability of surface pressure is small within a month, we use the climatology of surface pressure in July during each time period to calculate contours of enthalpy as a function of *Tmax* and RH (Figure 1). In each city and each time period, the cutoff curve roughly tracks a contour of constant enthalpy. As the maximum enthalpy is constrained, an increase in *Tmax* will induce a decrease of specific humidity at constant pressure according to Equation 7. These changes in *Tmax* and specific humidity both lead to a decrease in RH. What meteorological conditions control the local maximum enthalpy is still an open question and needs further work to quantitatively explain it, which is beyond the scope of this study. From 1990–2005 to 2071–2080, the cutoff shifts toward higher enthalpy contours and extends to lower RH. For instance, the cutoff in NYC is between enthalpy of 3 Megajoule/kg and 4 Megajoule/kg during 1990–2005, near 4 Megajoule/kg during 2026–2035, and approaches 5 Megajoule/kg during 2071–2080. This increase might be because global warming increases both the *Tmax* and the maximum moisture carrying capacity of air, thus permitting a higher maximum enthalpy at each location.

To test if these features are also shown in the observations, we examined the joint distribution of RH and *Tmax* at stations near the four selected grid cells (Figure S3). As we just have one climate realization for the observations, the station data (gray dots) are sparse. We used a period from 1980 to 2005 for the station data. This period is longer than the historical period 1990–2005 in the LENS simulations, which was a compromise between having more data and wanting to match the LENS historical period reasonably well. The general pattern for the joint distributions based on the HadISD station data is similar whether one uses observations during 1980–2005 or 1990–2005. As the locations of the four stations are either at an airport or in rural areas (Figure S1), observations in these stations are not representative of the city itself. In contrast, the data from LENS in a corresponding grid cell include a mixed signal calculated over both urban and rural surfaces. For this and other reasons, it is not a surprise that there are some biases in the joint distribution between RH and *Tmax* from LENS simulations compared to those from HadISD (Figure S3). Generally speaking, the RH and *Tmax* from both the HadISD observations and the LENS simulations present negatively dependent relationships that differ substantially across cities, with LENS correctly capturing the

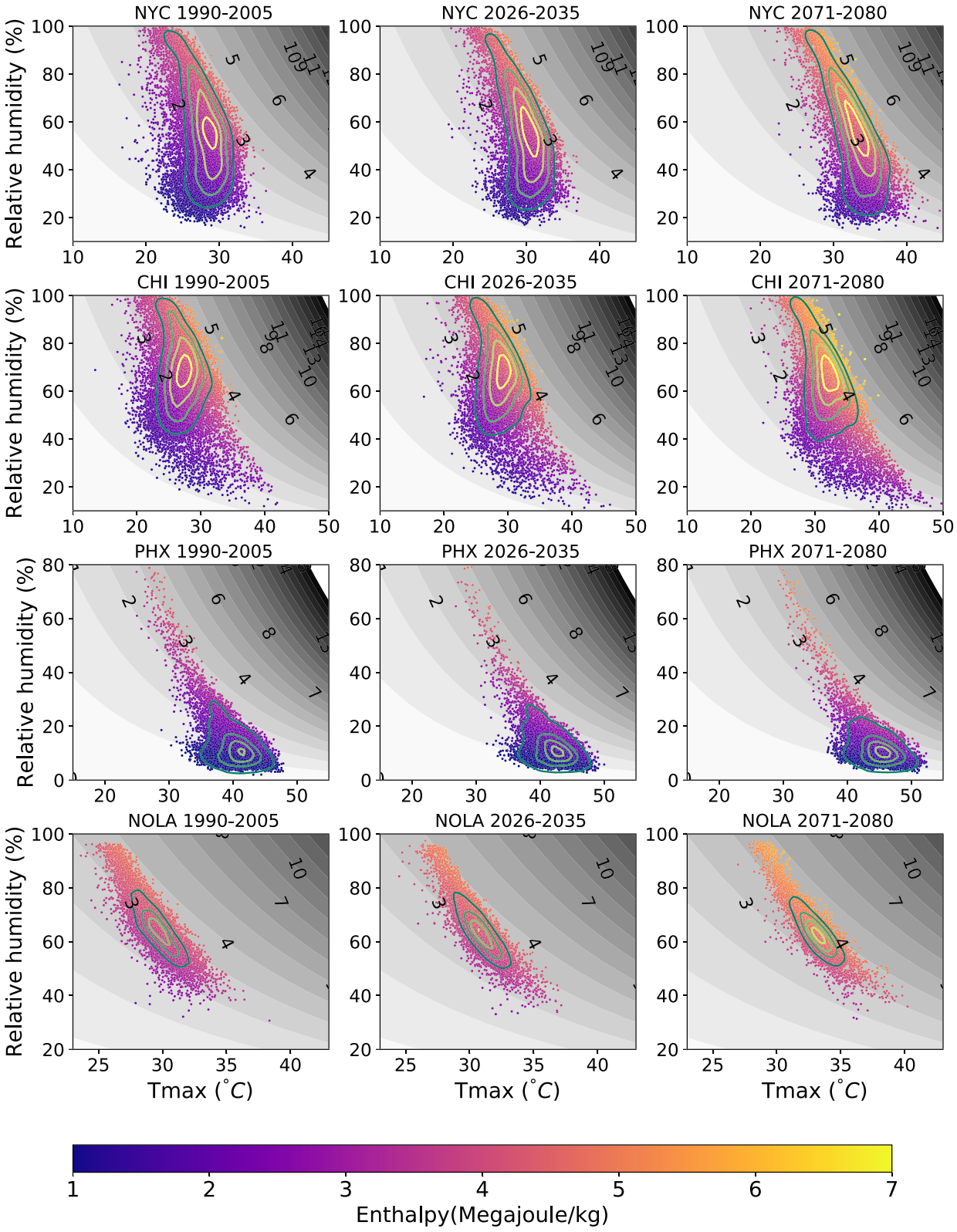

Figure 1. Joint distribution of RH and *Tmax* in July for three periods in (first row) New York (NYC), (second row) Chicago (CHI), (third row) Phoenix (PHX), and (fourth row) New Orleans (NOLA). Dots are simulated data of *Tmax* and RH from CESM LENS simulations. The color of dots denotes the value of enthalpy. Colored contours denote the density of dots, which increases as colors go from dark to light. Gray contours are the enthalpy calculated from RH, *Tmax* corresponding to the coordinate and the climatology of surface pressure in July over each period (units: Megajoule/kg).

larger differences in these relationships across the four cities, such as the high density of days with very warm temperature and low humidity in PHX (Figure S3). The correlation coefficients between the two variables are substantially negative in both HadISD and LENS for the four cities, with both observations and model output showing stronger anticorrelations in PHX and NOLA than in NYC and CHI (Table S2). These results indicate the LENS simulations can qualitatively capture the observed dependencies between RH and *Tmax* across these four locations. The focus of this study is on changes in the RH distribution conditional on *Tmax* from the historical to future periods, so we do not consider any bias corrections here. Given our focus on the cutoffs in the joint distribution between RH and *Tmax* simulated by LENS, it is encouraging to see reasonably clear cutoffs at the hot end of the joint distribution from the station data for all four cities, which suggests that these cutoffs are real physical phenomena.

In NYC and CHI, a kink is observed at the intersection of the cutoff curve and the cap at 100% RH. Above the temperature at the kink (T_0), the maximum RH decreases in a fairly linear fashion, and T_0 will be a parameter in our model for these cities. As the kinks only appear when there are RH values reaching 100% in the city, we select T_0 based on the *Tmax* when RH is close to 100% (see Appendix A for details).

4. Statistical Methodology

Standard parametric distributions cannot accurately capture the features of joint distributions between *Tmax* and RH, especially when a kink occurs. Here we construct conditional quantile regression models of RH|*Tmax* for each quantile. The quantile regression approach is applied to the joint distribution of RH and *Tmax* in July over the three periods, respectively. Based on the empirical characteristics of the joint distributions, we use two kinds of basis functions in the quantile regression models: One is a kink function to capture the kink when it is apparent in the joint distribution; the other is a set of cubic-spline basis functions of *Tmax*, which is used to capture smooth variation in RH as *Tmax* varies. Cubic splines in *Tmax* were used to flexibly model RH as a function of *Tmax* within a month. Our models for the τ^{th} quantile of RH|*Tmax* are of the form

$$\widehat{RH}_\tau(Tmax) = \theta + \gamma\,(Tmax - T_0)_+ + \sum_{j=1}^{m} \eta_j\, K_j(Tmax) \tag{9}$$

where T_0 is the temperature at the kink, $(Tmax - T_0)_+$ denotes the basis function that captures the kink, and $()_+$ is defined as

$$(x)_+ = \begin{cases} x, & x \geq 0 \\ 0, & x < 0 \end{cases}. \tag{10}$$

Here, θ is the intercept, γ and η_j are coefficients of basis functions, $K_j(Tmax)$ represents a cubic spline basis function, and m is the number of cubic spline basis functions. The metrics for selecting m and T_0 for each city are described in the appendix. The conditional quantile regression model estimates $\widehat{RH}_\tau$ at the specific quantile τ, so that the τ^{th} fraction of the residual differences between estimated RH ($\widehat{RH}_\tau$) and the simulated RH (RH_i) in LENS is positive, while the remaining $1-\tau$ fraction of residuals is negative. Mathematically, the quantile regression obtains the best estimates of the coefficients through solving the following minimization problem (Koenker & Bassett, 1978):

$$\tau \sum_{i=1}^{n} \left(RH_i - \widehat{RH}_\tau(Tmax_i)\right)_+ + (1-\tau) \sum_{i=1}^{n} \left(\widehat{RH}_\tau(Tmax_i) - RH_i\right)_+ \tag{11}$$

where $Tmax_i$ and RH_i indicate the observed value of a quantity on day i. $\widehat{RH}_\tau(Tmax_i)$ is the estimated quantile on day i, obtained by replacing $\theta,\gamma,\eta_{1,2,\ldots,m}$ by estimates that minimize the expression in 11.

The estimated quantiles produced by the quantile regression models closely match the variation of RH|*Tmax* in the simulated data from LENS for each period and city (Figure 2). These quantiles show the differences in RH as *Tmax* varies within a month, including the cutoff curve and the kink when it is present. Using the estimated quantiles of RH|*Tmax*, we can flexibly estimate distributions of multiple metrics that describe heat extremes, such as dew point and HI. There are some small spikes shown in the lines of low quantiles in some cities, for example, 0.5 quantiles during 2071–2080 in CHI. These spikes are due to overfitting by the kink

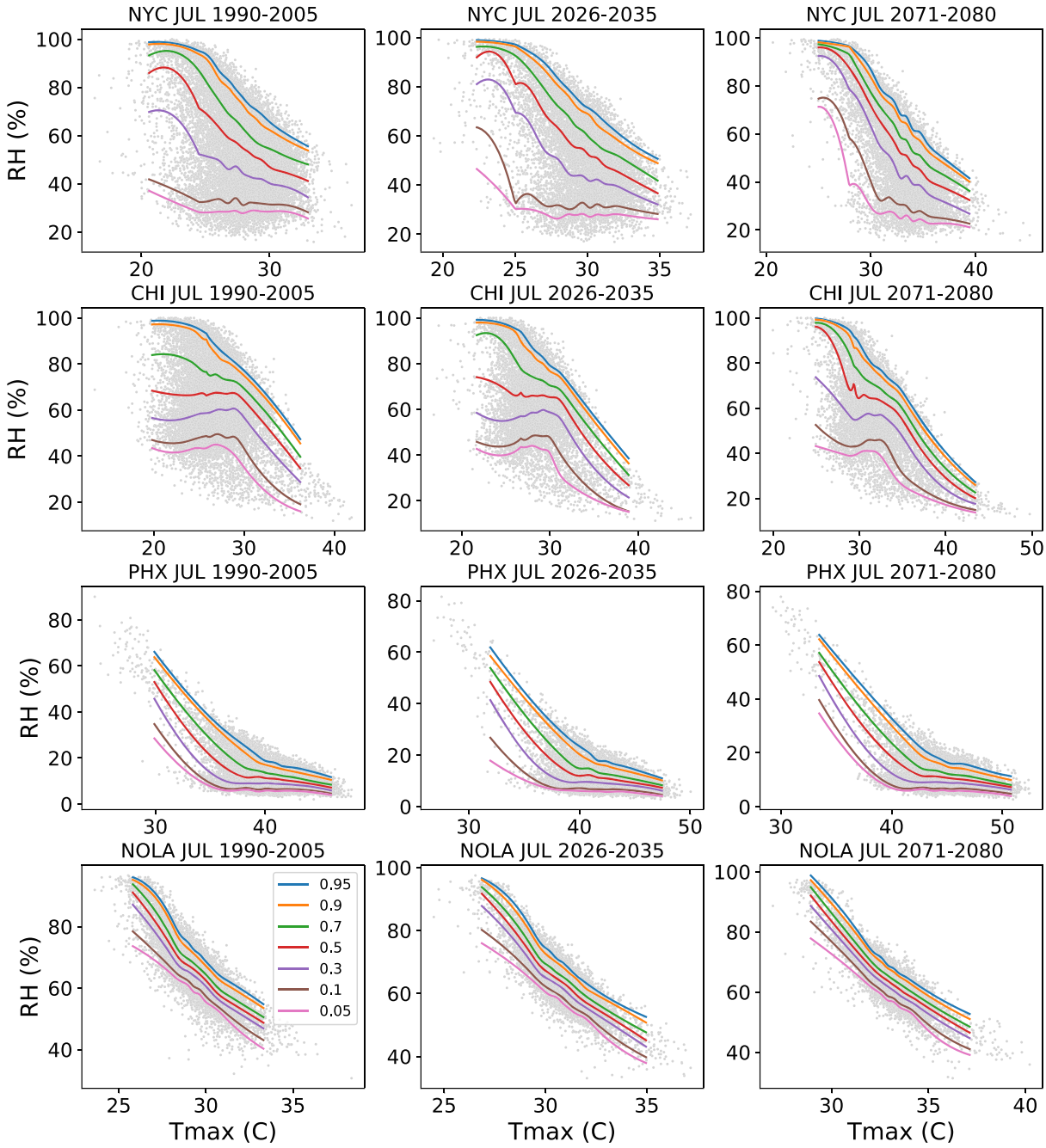

Figure 2. Estimated quantiles of RH|*Tmax* based on CESM LENS simulations in July of three periods at NYC (first row), CHI (second row), PHX (third row), and NOLA (fourth row). Gray dots are output of *Tmax* and RH from CESM LENS simulations. Lines represent the estimated quantiles at 0.05, 0.1, 0.3, 0.5, 0.7, 0.9, and 0.95.

function. As the spikes only appear in low quantiles that are not important for studies of extremes, we still use the kink function in the model as it is important for estimating the kink in high quantiles but recognize that these model specifications may not be optimal for all quantiles in all cities.

5. Model Validation

To evaluate how well the statistical model fits the simulated data in LENS (quality of fit), we perform cross validations and construct empirical inverse quantiles of the RH data in various temperature ranges. The quality of fit is evaluated as follows:

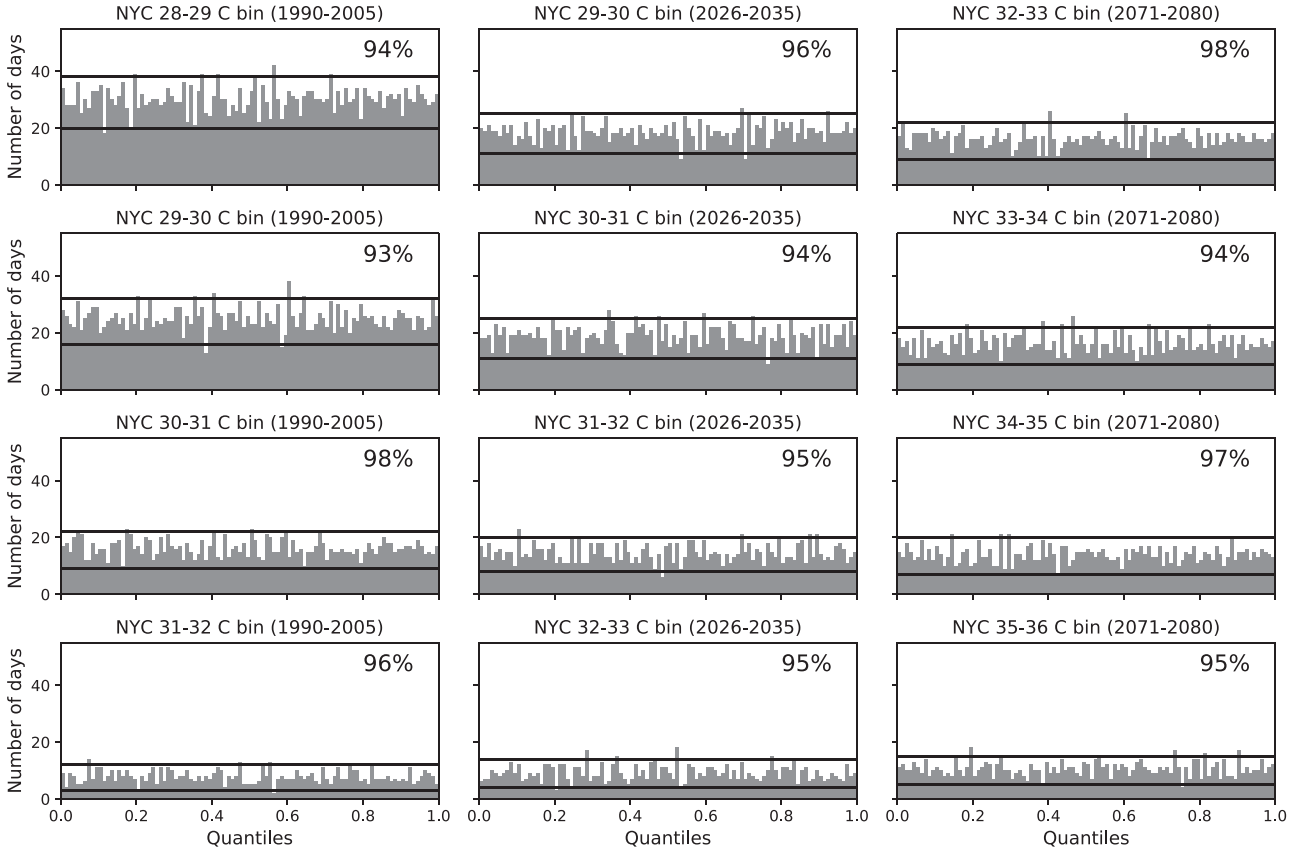

Figure 3. Inverse quantiles of the fitted statistical models compared to the empirical quantiles of simulated data in LENS in NYC during (first column) 1990–2005; (second column) 2026–2035; and (third column) 2071–2080. The histograms represent the number of RH events falling into 100 bins of estimated quantiles of RH at four given temperature intervals (1° per interval) in July. In a temperature interval, the solid line marks the 0.025 (lower bar) and 0.975 (upper bar) of the appropriate binomial distribution. The percentage at the upper right corner of each panel denotes the percentage of bins that has number of days falling in between the two bars.

1. We first predict the quantiles of RH given *Tmax* through a sevenfold cross-validation. Based on 35 members in LENS, we hold out 5 members a time and fit the quantile regression model to the remaining 30 members. Then the fitted model is used to predict 99 quantiles of the RH in the five hold-out members, from 0.01 to 0.99 and for the range of *Tmax* present in the data. We repeat this process seven times in which we select five hold-out members without replacement from the 35 members. In this manner, we obtained seven sets of $\widehat{RH}_\tau(Tmax)$ in 99 quantiles. The 99 quantiles will be used as boundaries of 100 bins between 0 and 1.
2. In each set, for temperature intervals of 1° width, we assign each day to an interval based on the value of *Tmax* for that day. For a particular temperature interval, the RH in these selected days are compared with the values of the 99 $\widehat{RH}_\tau(Tmax)$ quantiles and assigned to the corresponding RH quantile bins.
3. For each temperature interval, we combined the number of days assigned to each RH quantile bin across the seven holdout sets. The estimated quantiles of the corresponding RH in the temperature interval are displayed in a histogram to show the number of days falling into 100 bins from 0–0.01 quantile to 0.99–1 quantile (e.g., see Figure 3). The more uniform the histogram is, the better the quantile model fits the data.
4. To quantitatively evaluate the uniformity of the histograms in each temperature interval, we compared the number of days falling in each bin of a histogram with a binomial distribution. Under the assumption that *Tmax* and RH simulated by LENS in each day is independent and has the same probability of falling in each quantile bin, the number of days falling in each 0.01-quantile bin should be a binomial distribution with parameters n, the number of days falling in a temperature interval and p, the probability of falling in each quantile bin, which should equal 0.01 for each bin if our model is accurate. In a temperature interval, we pick the lower and upper bars (marked by black lines in Figure 3) based on the binomial

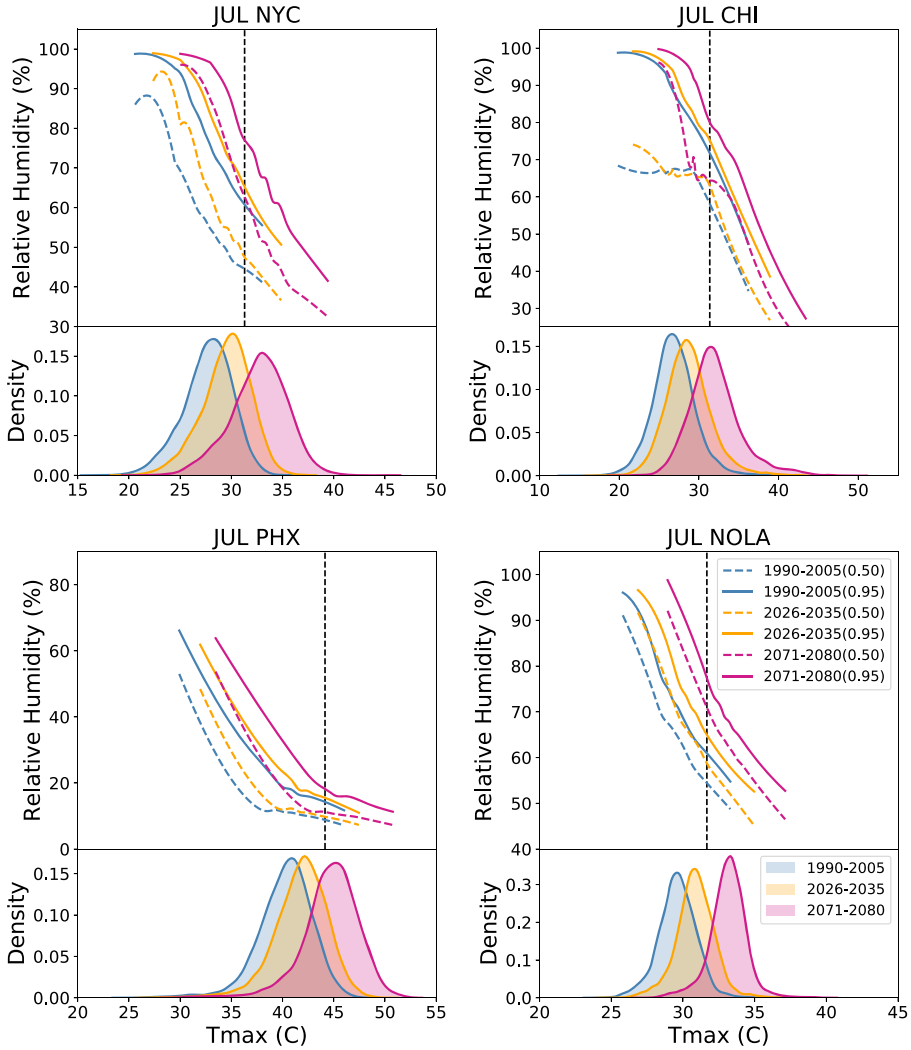

Figure 4. Estimated quantiles of relative humidity (RH) given daily maximum temperature (*Tmax*) in the three periods: 1990–2005, 2026–2036, and 2071–2080. Median and 0.95 quantiles are displayed by dashed and solid lines, respectively. Marginal distributions of temperature are shown in the lower panels. The dashed black lines denote the 0.95 quantiles of *Tmax* during the period of 1990–2005.

distribution to satisfy that if the true bin probability is 0.01, the probability of falling below the lower bar is at most 0.025, and the probability of falling above the upper bar is also at most 0.025. If the numbers of days in around 95% of bins are within the range of the upper and lower bars, the statistical model can be considered to fit the data well.

Taking NYC as an example (Figure 3), the simulated RH data from LENS are evenly distributed in the 100 bins edged by quantiles, which are estimated by the quantile regression models, given the selected temperature intervals for July in the three periods. For all selected temperature intervals, numbers of days in most of bins (close to 95% of the 100 bins) are within the 95% range of a Binomial(n, p) distribution with parameters n and $p = 0.01$. Similar features are observed in the other three cities (Figures S4–S6). These results indicate that the models we selected fit the data well for all four cities.

6. Results

To investigate the long-term evolution of heat extremes, we focus upon the conditional median of RH|*Tmax* and upon the conditional 0.95 quantile of RH|*Tmax*, which we take as representative of the tail of the conditional distribution (upper panels of Figure 4). As noted, the shape of the marginal *Tmax* distribution in

Table 1
Summary of Relative Humidity (RH), Dew Point (DP), and the Heat Index (HI) at 0.5 and 0.95 Quantiles in the Period of 1990–2005 (Denoted by Hist.) Given 0.5 and 0.95 Quantiles of Tmax in the Same Period

City	Tmax quantiles	Periods	*Tmax*	0.5 quantiles RH	0.5 quantiles DP	0.5 quantiles HI	0.95 quantiles RH	0.95 quantiles DP	0.95 quantiles HI
NYC	0.5	Hist.	27.9	54.9	18.0	28.8	76.0	23.3	31.3
		2030	1.8	−0.1	1.6	2.5	−3.2	1.0	3.6
		2075	5.0	−3.2	3.7	7.8	−8.2	2.9	11.0
	0.95	Hist.	31.3	44.6	17.8	32.1	60.7	22.8	35.7
		2030	1.8	−2.3	0.8	2.3	−3.9	0.6	2.9
		2075	5.6	−6.9	2.3	8.1	−10.8	2.0	9.8
CHI	0.5	Hist.	26.8	67.5	20.3	28.4	88.2	24.7	30.3
		2030	1.7	−1.7	1.2	2.7	−3.1	1.1	4.1
		2075	4.9	−3.2	3.8	9.3	−9.4	2.9	12.5
	0.95	Hist.	31.4	58.3	22.2	35.1	71.9	25.7	39.1
		2030	2.3	−9.3	−0.7	2.3	−8.4	0.2	3.7
		2075	6.8	−21.5	−1.4	7.2	−22.5	0.0	9.5
PHX	0.5	Hist.	40.5	11.1	4.5	37.5	18.3	11.9	39.6
		2030	1.5	0.0	1.1	1.6	−0.7	0.6	1.8
		2075	4.4	−0.3	2.9	4.8	−1.6	2.1	5.6
	0.95	Hist.	44.2	8.9	4.0	40.7	14.3	11.0	42.9
		2030	1.5	−0.1	1.1	1.6	−0.8	0.3	1.6
		2075	4.6	−0.1	3.2	4.7	−1.0	2.4	5.6
NOLA	0.5	Hist.	29.6	64.7	22.3	33.0	71.2	23.8	34.4
		2030	1.2	−1.2	0.9	2.4	−1.3	0.9	2.8
		2075	3.6	−2.5	2.8	8.0	−3.4	2.6	8.9
	0.95	Hist.	31.7	54.3	21.3	34.9	60.8	23.2	36.6
		2030	1.2	−0.6	0.9	2.2	−1.3	0.7	2.4
		2075	3.3	0.7	3.2	7.7	−0.5	2.9	8.4

Note. Each row labeled Hist. gives the values for this period. Other rows give changes from the historical period in *Tmax* (fourth column) and the conditional median of RH (Columns 5 and 8), DP (Columns 6 and 9) and HI (Columns 7 and 10) from the period Hist. to the period of 2026–2035 (rows labeled 2030) and to the period of 2071–2080 (rows labeled 2075) given the 0.5 and 0.95 quantiles of *Tmax* in the same period (units of *Tmax*: °C; units of RH: %; units of dew point: °C; units of HI: °C).

Table 2
Summary of Relative Humidity (RH), Dew Point (DP), and the Heat Index (HI) at the 0.95 and 0.5 Quantiles in the Period of 1990–2005 (Denoted by Hist.), Conditional Upon the 0.95 Quantile of Tmax During the Hist Period

City	Period	*Tmax*	0.95 quantiles RH	0.95 quantiles DP	0.95 quantiles HI	0.5 quantiles RH	0.5 quantiles DP	0.5 quantiles HI
NYC	Hist	31.3	60.8	22.8	35.7	44.5	17.8	32.1
	2030		+4.9	+1.2	+1.3	+3.4	+1.1	+0.6
	2075		+16.6	+4.1	+5.3	+17.7	+5.5	+4.1
CHI	Hist	31.4	71.9	25.6	39.1	58.3	22.2	35.1
	2030		+3.7	+0.8	+1.2	+5.1	+1.4	+1.3
	2075		+8.2	+1.9	+3.2	+6.2	+1.8	+1.9
PHX	Hist	44.2	14.4	11.0	43.0	9.0	4.1	40.8
	2030		+0.9	+1.0	+0.5	+0.8	+1.2	+0.3
	2075		+4.0	+3.8	+2.0	+2.4	+3.5	+1.0
NOLA	Hist	31. 7	60.8	23.2	36.6	54.3	21.3	34.9
	2030		+4.2	+1.1	+1.2	+4.5	+1.3	+1.1
	2075		+16.9	+4.1	+5.5	+16.9	+4.4	+4.9

Note. As in Table 1, rows labeled 2030 or 2075 show changes from the historical period, but now at a fixed temperature rather than a fixed quantile (units of *Tmax*: °C; units of changes in RH: %; units of changes in dew point: °C; units of changes in HI: °C).

each time period (lower panels of Figure 4) noticeably deviates from a normal distribution. Furthermore, the changes from the period 1990–2005 to the period 2071–2080 include not only increases in mean and changes in standard deviation but also changes in skewness and kurtosis. For example, in CHI in July, the mean increases from 26.9°C to 32.0°C, while the standard deviation grows from 2.7°C to 3.3°C. The skewness and kurtosis of *Tmax* also increase over time, indicating a more right-skewed and fatter tail distribution in the future climate. The changes in the marginal distribution of RH are smaller (Figure S7). The means of RH decrease in all cities (in a range between −0.02% and −3.20%), while changes in other moments of RH are not consistent across cities. The standard deviations of RH slightly increase in CHI, exhibit almost no change in NYC, and decrease in PHX and NOLA.

Two alternative ways of investigating RH|*Tmax* are to look at the change in RH at a fixed quantile of *Tmax* ($Tmax_\tau$; Tables 1) and to look at the change in RH at a fixed value of *Tmax* (Tables 2). The former is more representative of the overall shift in the joint distribution, while the latter is relevant to characterizing the heat stress of a day at a particular *Tmax*.

As expected, both $Tmax_{0.5}$ and $Tmax_{0.95}$ increase over time (Table 1). The conditional median of RH at the increasing $Tmax_{0.5}$ decreases over time in all cities, except for PHX between July 1990–2005 and 2026–2035, a period

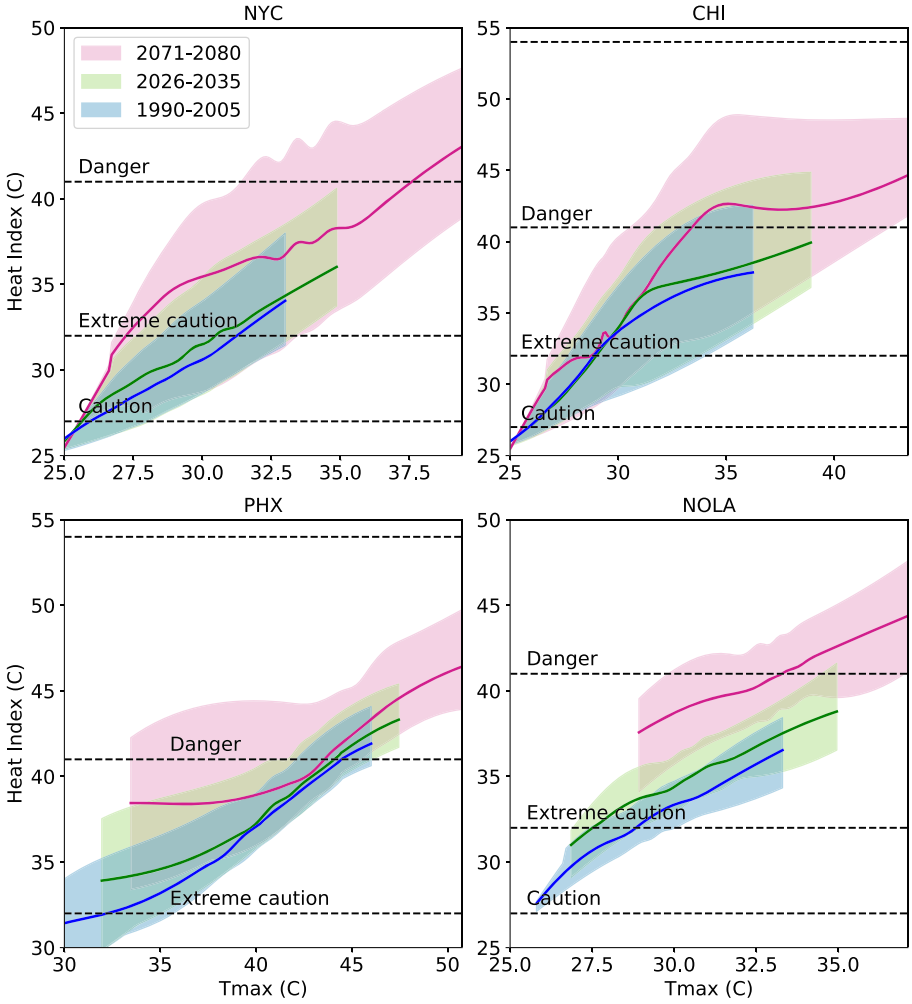

Figure 5. Estimated quantiles of the HI given daily maximum temperature (*Tmax*) in July for three periods in New York (NYC), Chicago (CHI), Phoenix (PHX), and New Orleans (NOLA). Shading represents the central 90% range of the distribution where blue, green, and red denote the 1990–2005, 2016–2035, and 2071–2080 periods, respectively. Heavy curves are the conditional medians of the distributions. The horizontal dashed lines denote the thresholds for heat index categories defined by the U.S. National Weather Service. Note that we should interpret the conditional HI distribution when *Tmax* > 50°C with caution in PHX during the 2071–2080.

over which the conditional median of RH is effectively constant. The same pattern holds for all four cities at $Tmax_{0.95}$, with the conditional median of RH decreasing over time (Table 1). The conditional 0.95 quantiles of RH on $Tmax_{0.5}$ and on $Tmax_{0.95}$ both decrease consistently over time in all four cities (Table 1). The projected decrease in the conditional median quantile of RH at a fixed quantile of *Tmax* indicates that the growth in saturation vapor pressure due to increased temperature is larger than the growth in the vapor pressure of the air. The result is consistent with findings in previous studies (Byrne & O'Gorman, 2018; Joshi et al., 2008; Kirtman et al., 2013; O'Gorman & Muller, 2010), which show a decrease in RH over land in response to a warming climate, as well as with the marginal decrease in mean RH noted early (Figure S7).

Given the increase in $Tmax_{0.5}$ and $Tmax_{0.95}$, the conditional median and 0.95 quantile of HI both increase in 2026–2035 and 2071–2080 relative to that in 1990–2005 (Table 1; Figure 5). The increase in HI in the two future periods is greater than the increase in $Tmax_{\tau}$ in most cities, except for PHX where the increase in HI is close to the increase in $Tmax_{\tau}$. The conditional median and 0.95 quantiles of dew point at both quantiles of *Tmax* increase over time except for conditional median quantiles in CHI, where the decrease in RH is large enough that there is a minimal change in conditional dew point (Table 1; Figure 6). This result suggests

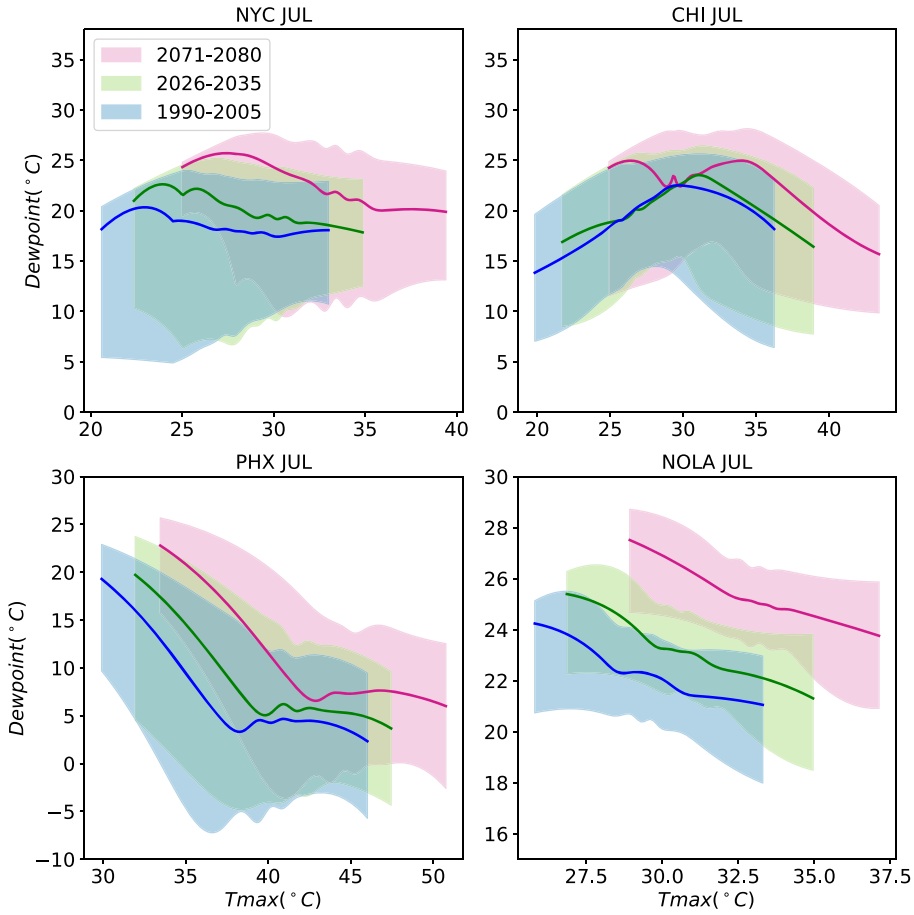

Figure 6. Estimated quantiles of dew point given daily maximum temperature (*Tmax*) in July of three periods at New York (NYC), Chicago (CHI), Phoenix (PHX), and New Orleans (NOLA). Shading represents the central 90% range of the distribution where blue, green, and red denote the 1990–2005, 2016–2035 and 2071–2080 periods, respectively. Heavy lines are conditional medians of the distributions.

that, despite a modest decrease in mean RH, heat stress considering both effects of temperature and humidity in a warming climate will increase faster than heat stress measured only by temperatures would indicate in many locations.

At a fixed value of *Tmax* (e.g., the 0.95 quantile of *Tmax* during 1990–2005), the conditional 0.95 quantiles of RH increase in all cities (upper panels of Figure 4 and Table 2). Changes in the conditional median quantiles of RH show similar patterns (Table 2). High and median conditional quantiles of HI and the dew point similarly display large increases over time in the four cities (Table 2; Figures 5 and 6). Our results suggest that, at a fixed extreme temperature, an increase in both the median and high quantiles of RH due to a warming climate will make people feel hotter in future days than in current days. In other words, heat stress on a day of a given temperature will, on average, be substantially worse in a warmer climate than heat stress on a day of the same temperature in the current climate.

We note that there are decreases in the dew point with increases in *Tmax* for each time period in all four cities (Figure 6). In addition, a peak of dew point is observed in CHI and NYC where the median dew point increases with *Tmax* up to a point and then decreases with further increases in *Tmax* for each time period. The *Tmax* at a peak of dew point is consistent with the *Tmax* at the kink in the corresponding RH quantiles. Since the dew point projections is mathematically transformed from the conditional quantiles of RH on *Tmax*, the decrease in the high quantiles of dew point along with the increase in *Tmax* at the hotter side of the peak reflects the cutoff of the RH distribution conditional on *Tmax* and the enthalpy constraint we discussed in section 3.

7. Discussions and Conclusions

In this study, we use a large ensemble of simulations to investigate the joint distribution of summertime RH and *Tmax* for three time periods (1990–2005, 2026–2035, and 2071–2080) in four U.S. cities that represent a range of climates. For July in each city, the joint distribution changes shape and shifts toward higher enthalpy values over time. A kink in the highest *Tmax* for which RH of 100% can occur, followed by a cutoff in the maximum attainable RH as *Tmax* increases beyond this kink, is observed in the joint distribution for NYC and CHI (Figure 1). The cutoff shifts toward a higher enthalpy as the climate warms.

Based on the information provided by the joint distribution diagnostics, we developed statistical models to capture the conditional distribution of RH|*Tmax* using quantile regression, where a kink function is used to capture the kink and a number of cubic spline basis functions are used to describe smooth variation in RH quantiles with *Tmax* within a month. The quality of fit diagnostic indicates that the distribution of RH|*Tmax* estimated by these quantile regression models fits the data of LENS well (Figures 3 and S4–S6). In addition, the quantile regression models could estimate the distribution and tails of the conditional distribution of RH|*Tmax* without any parametric assumptions on the shapes of the conditional distributions.

The conditional quantiles of RH|*Tmax* allow us to investigate the changes in heat extremes in multiple ways. First, we investigate the changes in RH, HI, and dew point given a fixed quantile of *Tmax* during any of the three periods. As expected, both $Tmax_{0.5}$ and $Tmax_{0.95}$ increase over time. At the $Tmax_{0.5}$ and $Tmax_{0.95}$ during future periods, the conditional quantiles of HI or dew point are generally higher than that during the historical period, even though the conditional quantiles of RH are lower (Table 1). These results suggest that, despite a modest decrease in RH, in a warming climate, heat stress considering both effects of temperature and humidity will tend to increase more than considering temperature alone would indicate.

Second, we investigate the changes in RH, HI, and dew point given a fixed *Tmax*. Fixing *Tmax* at its historical 0.95 quantile, for instance, the conditional 0.95 quantiles of RH, dew point and HI increase from 1990–2005 to 2071–2080 in all four cities (Table 2). This increasing pattern holds for the conditional median quantiles of these three variables given the fixed *Tmax* as well (Table 2). Our results indicate that, in a warming climate, a future day will tend to have higher RH than a day of the same temperature under the historic climate. Therefore, even at the same temperature, the increase in RH will increase the heat stress in the future day. Ignoring this conditional increase in RH, as some recent studies have done in assessing the heat impact (Carleton et al., 2020; Dosio et al., 2018; e.g. Mazdiyasni et al., 2017), may lead to underestimating the impact of heat waves in a warmer world.

This study gives us confidence about applying quantile regression models to quantify the conditional distribution of RH|*Tmax* in different climate backgrounds. For a specific city, although these statistical models capture the variability of RH given *Tmax* for a summer month and each time period, respectively, we see a need for a comprehensive model for all days throughout a year and all years throughout a long time period that could capture the seasonal variability and long-term evolution with the same set of parameters. To reach this end, we would need to include more terms in the statistical model to capture the variability of RH with time (e.g., days of the year and years) and the effect of any interactions between *Tmax* and time on RH.

Appendix A

A.1 Selecting the Temperature at the Kink

As discussed in the section 4, the kink is observed in cities where the RH can effectively reach 100%. Therefore, we use the following rule for deciding whether to include a kink function: First, we check if RH ever exceeds 99% in the city. If it does, then we include a kink function and obtain a value for T_0, which we set to the maximum *Tmax* in the days when RH is close to 100% (RH > 99%). This method for selecting T_0 follows our physical meaning of the kink as the maximum temperature at which RH can be nearly 100%. The selected T_0 values are listed in Table S1. To test if the quantile regression models are sensitive to the choice of T_0, we use multiple temperature values that are within a range of 3°C around the selected T_0 and apply each of them as T_0 in the model. The estimated quantiles based on the model with variate T_0 are similar with each other. However, the quantiles estimated by some models with T_0 value that are 0.5°C greater/less the T_0 we selected display unexpected curvature T_0 (Figures S8 and S9). This diagnostic gives us confidence that the T_0

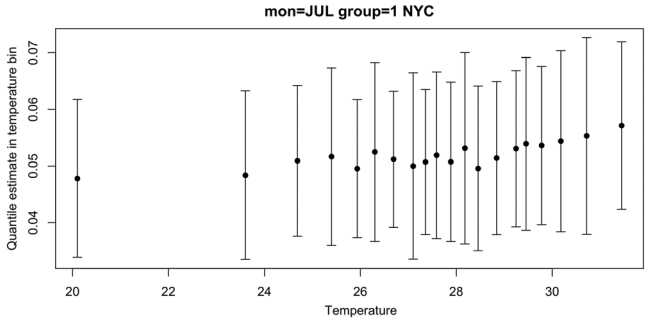

Figure A1. $\widehat{S}_{test}(a_j, \tau)$ in July of New York during period of 1990–2005 for the quantile $\tau = 0.95$ estimation. Twenty temperature bins are edged by equally spaced quantiles (0.05) from 0 to 1 of the *Tmax* distribution in July. The black dot and error bars indicate the mean and standard deviation in a temperature bin.

we selected generally captures the kink of the joint distribution in NYC and CHI, although more formal statistical methods may also work well.

A.2 Selecting Number of Basis Functions

The number of basis functions (m) in the model is an important parameter that influences how well the model fits the LENS outputs. Increasing m improves the quality of fit of the model. However, if m is too large, the model runs the risk of overfitting the data, which can lead to diminished performance in assessments in out-of-sample data. Here we use a cross-validation metric to select the simplest model that provides overall good estimation of quantiles and prevents overfitting the data.

To estimate the appropriate number of basis functions used in a quantile-regression model, we apply a cross validation on the model. We extract samples by randomly selecting 34 members from the 35 members of LENS and drop one member without replacement. By this way, we obtained 35 samples. Then, we apply quantile regression on each sample and calculate the fraction of RH events that exceeds a particular quantile τ given *Tmax* bins:

$$\widehat{S}_{test}(a_j, \tau) = \frac{1}{n}\sum_{i=1}^{n} I\left[\left(RH_i(a_j) - \widehat{RH}_{i,\tau}(a_j)\right) > 0\right] \tag{12}$$

where $n = 35$ is the number of samples. The a_j's represent temperature bins whose boundaries are defined by equally spaced quantiles (0.05) from 0 to 1 of the *Tmax* distribution in a month; RH_i represents the observed values from model output; $\widehat{RH}_{i,\tau}$ is the estimated value at quantile τ; and I is the indicator function. An appropriate model that is fit to the data requires the estimated quantiles to contain approximately the desired fraction of positive and negative residuals. Therefore, we seek a model that satisfies $\widehat{S}_{test}(a_j, \tau) \approx (1 - \tau)$. Figure A1 shows an example of $\widehat{S}_{test}(a_j, \tau)$ in July of NYC during the period 1990–2005 for the 0.95 quantile estimation. As we expected, the $\widehat{S}_{test}(a_j, \tau)$ at each temperature bin is generally close to 0.05.

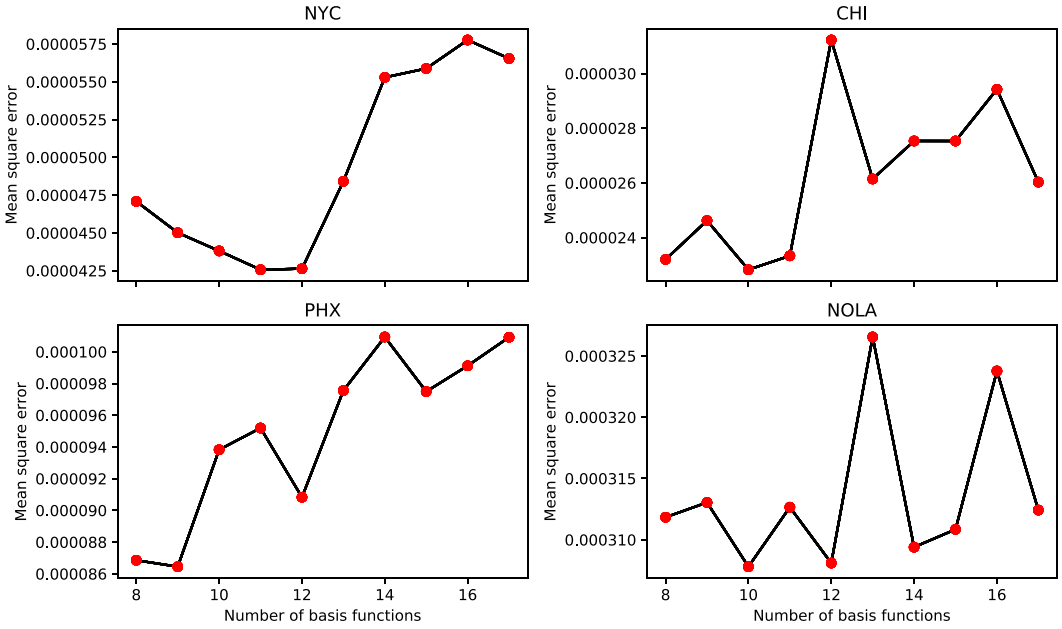

Figure A2. Averaged mean square error between $\widehat{S}_{test}(a_j, \tau)$ and 0.05 at estimated quantile $\tau = 0.95$ in July across three periods for New York (NYC), Chicago (CHI), Phoenix (PHX), and New Orleans (NOLA). Horizontal axis is the number of cubic-spline basis functions used in the statistical model.

The mean square error between $\widehat{S}_{test}(a_j,\tau)$ and 0.05 is used to measure the variability of $\widehat{S}_{test}(a_j,\tau)$. As the model complexity increases with the growth of m, the variability of $\widehat{S}_{test}(a_j,\tau)$ should decrease until reaching a minimum when m reaches an optimal number of basis functions. Once m exceeds this point, the model starts to overfit the data, and the mean square error between $\widehat{S}_{test}(a_j,\tau)$ and 0.05 will grow. For each city, we sum up the mean square error in July across three time periods:

$$CV = \frac{1}{3}\sum_{g=1}^{3}\frac{1}{k}\sum_{a_j=1}^{k}\left(\widehat{S}_{test}(a_j,\tau)_g - 0.05\right)^2 \tag{13}$$

where g represents three time periods. CV is used to quantify the averaged variability of $\widehat{S}_{test}(a_j)$ for a city (Figure A2). Based on Figure A2, the selected number of cubic-spline basis functions are 12 for NYC, 10 for CHI, 9 for PHX, and 10 for NOLA.

Data Availability Statement

The result data of this study are available in a repository online (https://doi.org/10.6084/m9.figshare.11283233.v2).

Acknowledgments

We would like to thank Anthony J. Broccoli, who provided inspiring discussion with Jiacan Yuan. This work was initiated from a class project. We would like to thank Joshua Couper, Nazia Arbab, Jessica August, and Sadiya Bab Tijjani for participating this project in the class of Statistics in Earth Science. The authors used the code developed by Joshua Couper to extract *Tmax* and corresponding RH from the LENS data. We acknowledge CESM Large Ensemble Community Project for providing us the LENS data. We also thank the Met Office Hadley Centre for providing HadISD data. Jiacan Yuan and Robert E. Kopp were supported by Rhodium Group as part of the Climate Impact Lab consortium. Robert E. Kopp has in the past served as a consultant to Rhodium Group. Jiacan Yuan was also supported by Shanghai Municipal Natural Science Fund (20ZR1407400). Michael L. Stein was supported by U.S. Department of Energy, Office of Science, Office of Advanced Scientific Computing Research (ASCR) under Contract DE-AC02-06CH11357.

References

Alduchov, O. A., & Eskridge, R. E. (1996). Improved Magnus form approximation of saturation vapor pressure. *Journal of Applied Meteorology*, *35*(4), 601–609. https://doi.org/10.1175/1520-0450(1996)035<0601:IMFAOS>2.0.CO;2

Allen, C. D., Macalady, A. K., Chenchouni, H., Bachelet, D., McDowell, N., Vennetier, M., et al. (2010). A global overview of drought and heat-induced tree mortality reveals emerging climate change risks for forests. *Forest Ecology and Management*, *259*(4), 660–684. https://doi.org/10.1016/j.foreco.2009.09.001

Basu, R., & Samet, J. M. (2002). Relation between elevated ambient temperature and mortality: A review of the epidemiologic evidence. *Epidemiologic Reviews*, *24*(2), 190–202. https://doi.org/10.1093/epirev/mxf007

Berry, I. L., Shanklin, M. D., & Johnson, H. D. (1964). Dairy shelter design based on milk production decline as affected by temperature and humidity. *Transactions of ASAE*, *7*(3), 329–331. https://doi.org/10.13031/2013.40772

Buzan, J. R., Oleson, K., & Huber, M. (2015). Implementation and comparison of a suite of heat stress metrics within the Community Land Model Version 4.5. *Geoscientific Model Development*, *8*(2), 151–170. https://doi.org/10.5194/gmd-8-151-2015

Byrne, M. P., & O'Gorman, P. A. (2016). Understanding decreases in land relative humidity with global warming: Conceptual model and GCM simulations. *Journal of Climate*, *29*(24), 9045–9061. https://doi.org/10.1175/JCLI-D-16-0351.1

Byrne, M. P., & O'Gorman, P. A. (2018). Trends in continental temperature and humidity directly linked to ocean warming. *Proceedings of the National Academy of Sciences*, *115*(19), 4863–4868. https://doi.org/10.1073/pnas.1722312115

Carleton, T. A., Jina, A., Delgado, M. T., Greenstone, M., Houser, T., Hsiang, S. M., et al. (2020). Valuing the global mortality consequences of climate change accounting for adaptation costs and benefits (Working Paper No. 27599). National Bureau of Economic Research. https://doi.org/10.3386/w27599

Collins, M., Knutti, R., Arblaster, J., Dufresne, J.-L., Fichefet, T., Friedlingstein, P., et al. (2013). Long-term climate change: Projections, commitments and irreversibility. In T. F. Stocker, et al. (Eds.), *Climate change 2013: The physical science basis. Contribution of working group I to the fifth assessment report of the Intergovernmental Panel on Climate Change* (pp. 1029–1136). Cambridge, UK and New York, NY, USA: Cambridge University Press.

Dai, A. (2006). Recent climatology, variability, and trends in global surface humidity. *Journal of Climate*, *19*(15), 3589–3606. https://doi.org/10.1175/JCLI3816.1

Dosio, A., Mentaschi, L., Fischer, E. M., & Wyser, K. (2018). Extreme heat waves under 1.5°C and 2°C global warming. *Environmental Research Letters*, *13*(5), 054006. https://doi.org/10.1088/1748-9326/aab827

Dunn, R. J. H., Willett, K. M., Thorne, P. W., Woolley, E. V., Durre, I., Dai, A., et al. (2012). HadISD: A quality-controlled global synoptic report database for selected variables at long-term stations from 1973–2011. *Climate of the Past*, *8*(5), 1649–1679. https://doi.org/10.5194/cp-8-1649-2012

Dunn, R. J. H., Mead, N. E., Willett, K. M., & Parker, D. E. (2014). Analysis of heat stress in UK dairy cattle and impact on milk yields. *Environmental Research Letters*, *9*(6), 064006. https://doi.org/10.1088/1748-9326/9/6/064006

Dunn, R. J. H., Willett, K. M., Ciavarella, A., & Stott, P. A. (2017). Comparison of land surface humidity between observations and CMIP5 models. *Earth System Dynamics*, *8*(3), 719–747. https://doi.org/10.5194/esd-8-719-2017

Fischer, E. M., & Knutti, R. (2013). Robust projections of combined humidity and temperature extremes. *Nature Climate Change*, *3*(2), 126–130. https://doi.org/10.1038/nclimate1682

Fischer, E. M., Oleson, K. W., & Lawrence, D. M. (2012). Contrasting urban and rural heat stress responses to climate change. *Geophysical Research Letters*, *39*, L03705. https://doi.org/10.1029/2011GL050576

Fontana, G., Toreti, A., Ceglar, A., & De Sanctis, G. (2015). Early heat waves over Italy and their impacts on durum wheat yields. *Natural Hazards and Earth System Sciences*, *15*(7), 1631–1637. https://doi.org/10.5194/nhess-15-1631-2015

Gibbins, C. J. (1990). A survey and comparison of relationships for the determination of the saturation vapour pressure over plane surfaces of pure water and of pure ice. *Annales Geophysicae (Berlin)*, *8*(12), 859–885.

Haugen, M. A., Stein, M. L., Moyer, E. J., & Sriver, R. L. (2018). Estimating changes in temperature distributions in a large ensemble of climate simulations using quantile regression. *Journal of Climate*, *31*(20), 8573–8588. https://doi.org/10.1175/JCLI-D-17-0782.1

Iribarne, J. V., & Godson, W. L. (1981). *Atmospheric thermodynamics*. Netherlands: Springer.

Joshi, M. M., Gregory, J. M., Webb, M. J., Sexton, D. M. H., & Johns, T. C. (2008). Mechanisms for the land/sea warming contrast exhibited by simulations of climate change. *Climate Dynamics*, *30*(5), 455–465. https://doi.org/10.1007/s00382-007-0306-1

Kay, J. E., Deser, C., Phillips, A., Mai, A., Hannay, C., Strand, G., et al. (2015). The Community Earth System Model (CESM) large ensemble project: A community resource for studying climate change in the presence of internal climate variability. *Bulletin of the American Meteorological Society*, *96*(8), 1333–1349. https://doi.org/10.1175/BAMS-D-13-00255.1

Kharin, V. V., Zwiers, F. W., Zhang, X., & Wehner, M. (2013). Changes in temperature and precipitation extremes in the CMIP5 ensemble. *Climatic Change*, *119*(2), 345–357. https://doi.org/10.1007/s10584-013-0705-8

Kirtman, B., Power, S. B., Adedoyin, J. A., Boer, G. J., Bojariu, R., Camilloni, I., et al. (2013). Near-term climate change: Projections and predictability. In T. F. Stocker, D. Qin, G.-K. Plattner, M. Tignor, S. K. Allen, J. Boschung, A. Nauels, Y. Xia, V. Bex, & P. M. Midgley (Eds.), *Climate Change 2013: The Physical Science Basis. Contribution of Working Group I to the Fifth Assessment Report of the Intergovernmental Panel on Climate Change* (pp. 953–1028). Cambridge, United Kingdom and New York, NY, USA: Cambridge University Press.

Kodra, E., & Ganguly, A. R. (2014). Asymmetry of projected increases in extreme temperature distributions. *Scientific Reports*, *4*(1), 5884. https://doi.org/10.1038/srep05884

Koenker, R., & Bassett, G. (1978). Regression quantiles. *Econometrica*, *46*(1), 33–50. https://doi.org/10.2307/1913643

Koenker, R., & Hallock, K. F. (2001). Quantile regression. *Journal of Economic Perspectives*, *15*(4), 143–156. https://doi.org/10.1257/jep.15.4.143

Lawrence, M. G. (2005). The relationship between relative humidity and the dewpoint temperature in moist air—A simple conversion and applications. *Bulletin of the American Meteorological Society*, *86*(2), 225–234. https://doi.org/10.1175/BAMS-86-2-225

Li, D., Yuan, J., & Kopp, R. (. B.). (2020). Escalating global exposure to compound heat-humidity extremes with warming. *Environmental Research Letters*, *15*(6), 064003. https://doi.org/10.1088/1748-9326/ab7d04

Masterton, J. M., & Richardson, F. A. (1979). *Humidex: A method of quantifying human discomfort due to excessive heat and humidity*. Downsview, Ontario, Canada: Environment Canada, Atmospheric Environment.

Matthews, T. (2018). Humid heat and climate change. *Progress in Physical Geography: Earth and Environment*, *42*(3), 391–405. https://doi.org/10.1177/0309133318776490

Mazdiyasni, O., AghaKouchak, A., Davis, S. J., Madadgar, S., Mehran, A., Ragno, E., et al. (2017). Increasing probability of mortality during Indian heat waves. *Science Advances*, *3*(6), e1700066. https://doi.org/10.1126/sciadv.1700066

Meehl, G. A., & Tebaldi, C. (2004). More intense, more frequent, and longer lasting heat waves in the 21st century. *Science*, *305*(5686), 994–997. https://doi.org/10.1126/science.1098704

Mora, C., Dousset, B., Caldwell, I. R., Powell, F. E., Geronimo, R. C., Bielecki, C. R., et al. (2017). Global risk of deadly heat. *Nature Climate Change*, *7*(7), 501–506. https://doi.org/10.1038/nclimate3322

Moran, D. S., Pandolf, K. B., Shapiro, Y., Heled, Y., Shani, Y., Mathew, W. T., & Gonzalez, R. R. (2001). An environmental stress index (ESI) as a substitute for the wet bulb globe temperature (WBGT). *Journal of Thermal Biology*, *26*(4–5), 427–431. https://doi.org/10.1016/S0306-4565(01)00055-9

O'Gorman, P. A., & Muller, C. J. (2010). How closely do changes in surface and column water vapor follow Clausius-Clapeyron scaling in climate change simulations? *Environmental Research Letters*, *5*(2), 025207. https://doi.org/10.1088/1748-9326/5/2/025207

Oleson, K. W., Monaghan, A., Wilhelmi, O., Barlage, M., Brunsell, N., Feddema, J., et al. (2013). Interactions between urbanization, heat stress, and climate change. *Climatic Change*, *129*(3–4), 525–541. https://doi.org/10.1007/s10584-013-0936-8

Orlowsky, B., & Seneviratne, S. I. (2012). Global changes in extreme events: Regional and seasonal dimension. *Climatic Change*, *110*(3-4), 669–696. https://doi.org/10.1007/s10584-011-0122-9

Papalexiou, S. M., AghaKouchak, A., Trenberth, K. E., & Foufoula-Georgiou, E. (2018). Global, regional, and megacity trends in the highest temperature of the year: Diagnostics and evidence for accelerating trends. *Earth's Future*, *6*(1), 71–79. https://doi.org/10.1002/2017EF000709

Ramamurthy, P., Li, D., & Bou-Zeid, E. (2017). High-resolution simulation of heatwave events in New York City. *Theoretical and Applied Climatology*, *128*(1–2), 89–102. https://doi.org/10.1007/s00704-015-1703-8

Rothfusz, L. P. (1990). The Heat Index "equation" (or, more than you ever wanted to know about heat index). In *Tech. Attachment* (Vol. 1, pp. 1–2). TX. 90-23

Russo, S., Sillmann, J., & Sterl, A. (2017). Humid heat waves at different warming levels. *Scientific Reports*, *7*(1), 7477–7477. https://doi.org/10.1038/s41598-017-07536-7

Sriver, R. L., Forest, C. E., & Keller, K. (2015). Effects of initial conditions uncertainty on regional climate variability: An analysis using a low-resolution CESM ensemble. *Geophysical Research Letters*, *42*, 5468–5476. https://doi.org/10.1002/2015GL064546

Steadman, R. G. (1979a). The assessment of sultriness. Part I: A temperature-humidity index based on human physiology and clothing science. *Journal of Applied Meteorology*, *18*(7), 861–873. https://doi.org/10.1175/1520-0450(1979)018<0861:TAOSPI>2.0.CO;2

Steadman, R. G. (1979b). The assessment of sultriness. Part II: Effects of wind Extra Radiation and Barometric Pressure on Apparent Temperature. *Journal of Applied Meteorology*, *18*(7), 874–885. https://doi.org/10.1175/1520-0450(1979)018<0874:TAOSPI>2.0.CO;2

Stocker, T. F., Qin, D., Plattner, G. K., Tignor, M., Allen, S. K., Boschung, J., et al. (2013). *Climate Change 2013: The Physical Science Basis. Contribution of Working Group I to the Fifth Assessment Report of the Intergovernmental Panel on Climate Change* (pp. 1–1535). Cambridge, UK and New York, NY, USA: Cambridge University Press.

Subin, Z. M., Riley, W. J., & Mironov, D. (2012). An improved lake model for climate simulations: Model structure, evaluation, and sensitivity analyses in CESM1. *Journal of Advances in Modeling Earth Systems*, *4*, M02001. https://doi.org/10.1029/2011MS000072

Sutton, R. T., Dong, B., & Gregory, J. M. (2007). Land/sea warming ratio in response to climate change: IPCC AR4 model results and comparison with observations. *Geophysical Research Letters*, *34*, L02701. https://doi.org/10.1029/2006GL028164

Tebaldi, C., Hayhoe, K., Arblaster, J. M., & Meehl, G. A. (2006). Going to the extremes. *Climatic Change*, *79*(3–4), 185–211. https://doi.org/10.1007/s10584-006-9051-4

Thom, E. C. (1958). Cooling degree days air Cond. *Heat. Vent.*, *55*, 65–69.

van Vuuren, D. P., Edmonds, J., Kainuma, M., Riahi, K., Thomson, A., Hibbard, K., et al. (2011). The representative concentration pathways: An overview. *Climatic Change*, *109*(1–2), 5–31. https://doi.org/10.1007/s10584-011-0148-z

Willett, K. M., Berry, D. I., Bosilovich, M. G., & Simmons, A. J. (2018). Surface humidity [in "state of the climate in 2018"]. *Bulletin of the American Meteorological Society*, *100*(9), Si–S306. https://doi.org/10.1175/2019BAMSStateoftheClimate.1

Willett, K. M., Dunn, R. J. H., Thorne, P. W., Bell, S., de Podesta, M., Parker, D. E., et al. (2014). HadISDH land surface multi-variable humidity and temperature record for climate monitoring. *Climate of the Past*, *10*(6), 1983–2006. https://doi.org/10.5194/cp-10-1983-2014

Willett, K. M., & Sherwood, S. (2012). Exceedance of heat index thresholds for 15 regions under a warming climate using the wet-bulb globe temperature. *International Journal of Climatology*, *32*(2), 161–177. https://doi.org/10.1002/joc.2257

Yaglou, C. P., & Minard, D. (1957). Control of heat casualties at military training centers. *Archives of Industrial Health*, *16*(4), 302–316.

Yano, J.-I., & Ambaum, M. H. P. (2017). Moist static energy: Definition, reference constants, a conservation law and effects on buoyancy. *Quarterly Journal of the Royal Meteorological Society*, *143*(708), 2727–2734. https://doi.org/10.1002/qj.3121

Zuo, J., Pullen, S., Palmer, J., Bennetts, H., Chileshe, N., & Ma, T. (2015). Impacts of heat waves and corresponding measures: A review. *Journal of Cleaner Production*, *92*, 1–12. https://doi.org/10.1016/j.jclepro.2014.12.078